Journal of Korean Society of
Coastal and Ocean Engineers
Vol. 13, No. 1, pp. 1~8, March 2001

2-DH Quadtree based Modelling of Longshore Current
연안류에 대한 2D-H 사면구조에 기초한 수치모델링

Koo-Yong Park*
박 구 용*

Abstract □ Wave-induced currents drive nearshore transport processes, and hence an accurate understanding of wave-current interaction is required for proper management of coastal zone. This paper presents details of an adaptive quadtree grid based numerical model of the coupled wave climate and depth-averaged current field. The model accounts for wave breaking, shoaling, refraction, diffraction, wave-current interaction, set-up and set-down, mixing processes, bottom friction effects, and movement of land-water interface at the shoreline. The wave period- and depth-averaged governing equations are discretized explicitly by means of an Adams-Bashforth second-order finite difference technique on adaptive hierarchical staggered quadtree grids. Results from the numerical model are in reasonable agreement with the laboratory data of longshore current generated by oblique waves on a plane beach (Visser 1980, 1991).

Keywords : wave-induced longshore current, wave-current interaction, nearshore hydrodynamics, quadtree

要 旨 : 파랑으로 인해 발생되는 흐름은 연안에서 질량수송의 일련의 과정을 야기시키므로 연안유역의 관리에 파랑과 흐름의 상호작용에 대한 정확한 이해가 요구된다. 본 논문은 적응가능한 사면 구조 격자에 근간을 둔 파랑장과 흐름장을 혼합한 수치모델을 기술하였다. 사용한 모델은 쇄파, 천수, 굴절, 회절, 파랑과 흐름의 상호작용, 평균해면의 저하와 상승, 혼합 과정, 바닥 마찰 효과 그리고 해안선에 접한 운동 등을 해석할 수 있다. 주기와 수심으로 평균한 지배 방적식은 단계적으로 엇갈린 사면구조 격자에 적용 가능한 Adam-Bashforth 2차 유한 차분 기법으로 양해적으로 모델화되었다. 본 모델로부터의 결과는 평면 해변에서 경사 입사파에 의해 발생된 연안류의 실험치와 타당한 일치를 보였다.

핵심용어 : 연안류, 파랑과 흐름의 상호작용, 연안 수동력학, 사면구조 격자

1. INTRODUCTION

Theoretical models of nearshore hydrodynamics are increasingly used by coastal engineers and scientists to simulate wave climate and induced currents, that in turn affects and transport and effluent dispersion. Much research effort has been applied over the past 25 years to the numerical modeling of nearshore wave-current interaction over relatively large coastal domains using depth- and wave period-averaged mathematical formulations of the mass, momentum, wave energy and wave number conservation relations. Examples include the models developed by Birkemeier *et al.* (1976), Ebersole and Dalrymple (1980) and Yoo and O'Connor (1986). Almost all such numerical solvers are based on a structured grid system comprising either fixed rectangular grids or uniform curvilinear boundary-fitted grids. But it is not computationally efficient for the grid to be of uniformly high resolution throughout the entire numerical domain. Un-structured advancing front or Voronoï grids have been used for approximating complicated geometries and can be readily adapted. However, the computations can be expensive because the nodal index system is extremely complicated, and nodal reordering may be required to make the solution matrix less sparse.

Herein, adaptive hierarchical grids based on quadtrees

*현대건설 토목설계실(Civil Design Section, Hyundai Eng. & Con. Co., Chongro-Ku, Seoul 110-793, Korea)

are applied to the modeling of nearshore hydrodynamics. Quadtree grids maintain straightfor-ward nodal connectivity through the tree structure, even though the grids may be highly non-uniform, and being based on recursive spatial decomposition. These are robust, automatic and efficient to generate quadtree mesh system (see Yiu *et al.* 1996).

This paper describes a period- and depth-averaged 2DH numerical model of wave-current interaction based on adaptive quadtree grids, where spatial discretization is formed by finite differences. An explicit Adams-Bashforth second-order scheme is used for time integration. Grid adaptation is achieved using seeding points according to local current gradient criteria.

2. QUADTREE GRID GENERATION

Quadtree techniques have been applied to a great variety of engineering problems since they were first used in image processing by Samet (1982). From a numerical modeling point of view, quadtree grids are generally cheaper and easier to adapt to very complicated domains than either curvilinear grids or unstructured meshes. Yiu *et al.* (1996) and Greaves and Borthwick (1999) describe typical methodologies for creating quadtree grids. The essence of quadtree grid generation is as follows. The domain of interest is normalized to fit within a unit square. The square is initially subdivided into four quadrants. Each cell is then subdivided into four smaller cells of equal sizes, and this process is recursively repeated according to criteria such as the presence of boundary seeding points in a cell, or the magnitude of representative physical variables (e.g. the gradients of depth-averaged current velocities).

After the first stage of grid generation, the resulting grid often contains adjacent cells of different sizes with hanging nodes at the interface edges. A hanging node occurs where the vertex of one cell coincides with an edge of a neighbor cell and adjacent cells are more than one level apart in the quadtree. It should be noted that care has to be taken to ensure that conservation requirements are not violated when applying numerical approximations to the governing partial differential equations at hanging nodes.

For any arbitrary cell in the quadtree grid, its neighbor cells can be identified by examining the branching structure of the quadtree system and determining the relative cell paths up the tree to the root cell (i.e. unit square). A linked list method is used herein due to its use of memory pointers for efficient data accessing (Yiu *et al.* 1996). Each link has pointers from the object cell to its parent cell and its subdivided child cells. Hence every cell can be identified by systematically searching the quadtree in the tree path. The concept of *Nearest Common Ancestor* (NCA) is used to find the neighbor of any given object cell. *NCA* is the smallest branching cell that is shared by the object cell and the neighbor under consideration. Further details of the cell numbering system and neighbor finding algorithms used here are given by Yiu *et al.* (1996) and Park (1999).

3. GOVERNING EQUATIONS

The depth- and wave period-averaged wave energy, wave conservation, mass and momentum conservation governing equations are after Yoo and O'Connor (1986) as follows :

$$\frac{\partial \eta}{\partial t} + \frac{\partial}{\partial x_i}(dU_i) = 0 \tag{1}$$

$$\frac{\partial U_i}{\partial t} + U_j\frac{\partial U_i}{\partial x_j} + \frac{1}{\rho d}\frac{\partial S_{ij}}{\partial x_j} + g\frac{\partial \eta}{\partial x_i} - \frac{\tau_{wi} - \tau_{bi}}{\rho d} - \frac{\partial}{\partial x_j}\left(\varepsilon_j \frac{\partial U_i}{\partial x_j}\right) = 0 \tag{2}$$

$$\frac{\partial K_i}{\partial t} + (Cg_i + U_j)\frac{\partial K_i}{\partial x_j} + S_h\frac{\partial d}{\partial x_i} + K_j\frac{\partial U_i}{\partial x_i} - \frac{Cg}{2ka}\frac{\partial^3 a}{\partial x_i \partial x_j^2} = 0 \tag{3}$$

$$\frac{\partial a}{\partial t} + \frac{1}{2a}\frac{\partial}{\partial x_i}\{(Cg_i + U_i)a^2\} + \frac{S_{ij}}{\rho g a}\frac{\partial U_j}{\partial x_i} + C^a a^2 - \frac{1}{2}\frac{K_i}{K^2}\frac{\partial}{\partial x_j}\left(\varepsilon_j \frac{\partial}{\partial x_j} K_i a\right) = 0 \tag{4}$$

where $i, j = 1, 2$ are in tensor notation and correspond to x- and y-components, K is a component of the local wave number vector, U is the current velocity component, S_h is the depth variation factor, a is the wave amplitude, d is the depth, Cg is the group celerity of the waves, t is time and x is a cartesian spatial coordinate, η is the period-averaged surface elevation, g is the acceleration due to gravity, τ_w is surface wind stress, τ_b is bed friction stress and ε is the eddy mixing coefficient. The friction coefficient C^a is determined using Bijker's (1966) empirical formula. Thornton's (1970) algebraic formula is used herein to estimate ε. Wave breaking is treated using empirical

criteria, such as the US-CERC (1984) formula. The radiation stress tensor may be written

$$S_{ij} = \frac{1}{2}\left[(1+\delta)(1+G)\frac{K_i K_j}{K K} + G\delta_{ij}\right]\left(\frac{1}{2}\rho g a^2\right) \tag{5}$$

in which δ is the diffraction factor, $G = 2kd/\sinh 2kd$, δ_{ij} is the Kronecker delta, k is the wave number, and ρ is the water density.

4. NUMERICAL MODEL

The quadtree grid can have up to 49 possible cell configurations (as shown by Park, 1999), some of which are related through reflection or rotation. Spatial discretization was carried out on a simple uniform grid template by linear interpolation where necessary, according to the local cell configuration.

The second-order accurate Adams-Bashforth time-stepping algorithm is used, such that

$$\phi_P^{n+1} = \phi_P^n + \Delta t\left(\frac{3}{2}\frac{\partial\phi}{\partial t}\Big|_P^n - \frac{1}{2}\frac{\partial\phi}{\partial t}\Big|_P^{n-1}\right) \tag{6}$$

where $\phi = E$, K_i, K_j, η, U_i and U_j depending on the equation being solved. The superscript n is a time index, so that $t = n\Delta t$. Note that Δt is the time step. The subscript P indicates that (6) is cell-centred for (1) and (4), the east face for x-direction of (2) and (3) and the north face for y-direction of (2) and (3). The variables on uniformed mesh is shown in the Fig. 1.

For example, x-direction momentum equation is (see Fig. 2)

$$U_{C'}^{n+1} = U_{C'}^n + \Delta t\left(\frac{3}{2}\frac{\partial U}{\partial t}\Big|_{C'}^n - \frac{1}{2}\frac{\partial U}{\partial t}\Big|_{C'}^{n-1}\right) \tag{7}$$

where

$$\frac{\partial U}{\partial t}\Big|_{C'} = -\Delta t\left\{U_{C'}\frac{\partial U}{\partial x}\Big|_{C'} + V_{C'}\frac{\partial U}{\partial y}\Big|_{C'} - \frac{\tau_{wxC'} - \tau_{bxC'}}{\rho d_{C'}} + \frac{1}{\rho d_{C'}}\left[\frac{S_{xyE'} - S_{xyW'}}{\Delta x} + \frac{S_{yyN'} - S_{yyS'}}{\Delta y}\right] + g\frac{\eta_{E'} - \eta_{W'}}{\Delta x} - \left(\varepsilon_{xC'}\frac{4U_{E'} - 8U_{C'} + 4U_{W'}}{\Delta x^2} + \varepsilon_{yC'}\frac{4U_{N'} - 8U_{C'} + 4U_{S'}}{\Delta y^2}\right)\right\}$$

in which

$$\frac{\partial U}{\partial x}\Big|_{C'} = \begin{cases} \dfrac{U_{C'} - U_{WW'}}{\Delta x} & \text{if } V_{C'} > 0 \\ \dfrac{U_{EE'} - U_{C'}}{\Delta x} & \text{if } V_{C'} \le 0 \end{cases} \tag{8}$$

and

$$\frac{\partial U}{\partial y}\Big|_{C'} = \begin{cases} \dfrac{U_{C'} - U_{SS'}}{\Delta y} & \text{if } U_{C'} > 0 \\ \dfrac{U_{NN'} - U_{C'}}{\Delta y} & \text{if } U_{C'} \le 0 \end{cases} \tag{9}$$

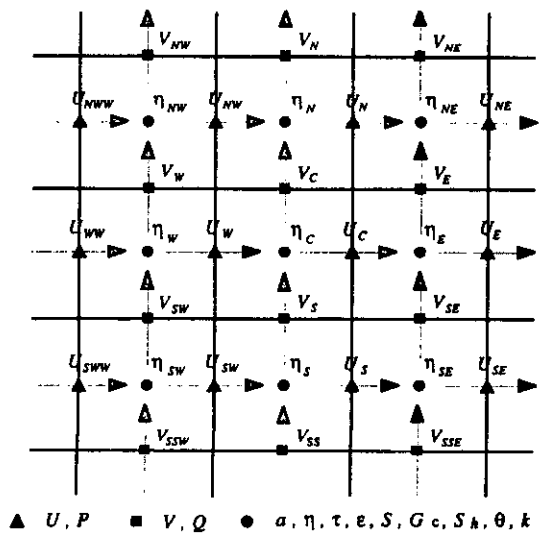

Fig. 1. Variables on staggered uniformed quadtree grid.

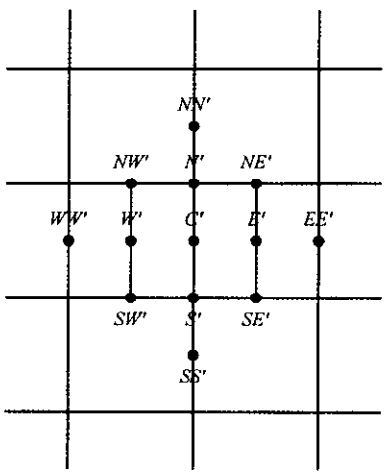

Fig. 2. Discretized x-direction current and wave number on uniform quadtree template.

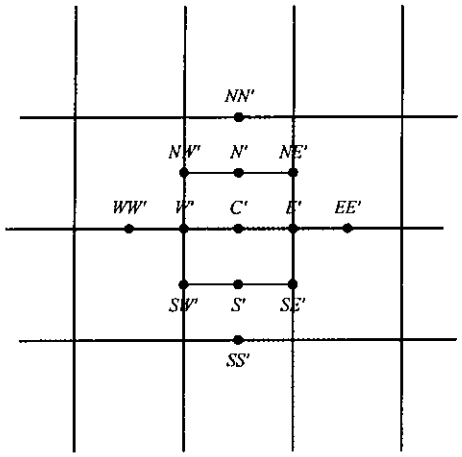

Fig. 3. Discretized y-direction current and wave number on uniform quadtree template.

From the linear interpolation (other governing equations with each cell configuration are followed under the same procedures, details are given in Park (1999)),

$$
\begin{aligned}
&U_{E*} = (U_C + U_E)/2,\ U_{W*} = (U_W + U_C)/2,\\
&U_{N*} = (U_N + U_C)/2,\ U_{S*} = (U_S + U_C)/2,\\
&U_{C*} = U_C,\ U_{WW*} = U_W,\ U_{EE*} = U_E,\ U_{SS*} = U_S,\ U_{NN*} = U_N,\\
&\eta_{E*} = \eta_E,\ \eta_{W*} = \eta_C,\ V_{C*} = (V_E + V_S)/2,\\
&d_{C*} = (d_C + d_E)/2,\ S_{xxE*} = S_{xxE},\ S_{xxW*} = S_{xxC},\\
&S_{xyN*} = (S_{xyN} + S_{xyE})/2,\ S_{xyS*} = (S_{xyS} + S_{xyE})/2,\\
&\tau_{wxC*} = (\tau_{wxC} + \tau_{wxE})/2,\ \tau_{bxC*} = (\tau_{bxC} + \tau_{bxE})/2,\\
&\text{and } \varepsilon_{xC} = (\varepsilon_{xC} + \varepsilon_{xE})/2,\ \varepsilon_{yC*} = (\varepsilon_{yC} + \varepsilon_{yE})/2
\end{aligned}
\tag{10}
$$

With reference to the uniform quadtree grid configuration in Fig. 3, the quadtree finite difference form of the y-direction momentum equation is

$$
V_{C'}^{n+1} = V_{C'}^{n} + \Delta t\left(\frac{3}{2}\frac{\partial V}{\partial t}\bigg|_{C'}^{n} - \frac{1}{2}\frac{\partial V}{\partial t}\bigg|_{C'}^{n-1}\right) \tag{11}
$$

where

$$
\begin{aligned}
\frac{\partial V}{\partial t}\bigg|_{C'} = -\Delta t\Bigg\{ & U_{C'}\frac{\partial V}{\partial x}\bigg|_{C'} + V_{C'}\frac{\partial V}{\partial y}\bigg|_{C'} - \frac{\tau_{wxC'} - \tau_{bxC'}}{\rho d_{C'}}\\
& + \frac{1}{\rho d_C}\left[\frac{S_{xyE'} - S_{xyW'}}{\Delta x} + \frac{S_{yyN'} - S_{yyS'}}{\Delta y}\right] + g\frac{\eta_{N'} - \eta_{S'}}{\Delta y}\\
& - \left(\varepsilon_{xC}\frac{4U_{E'} - 8U_{C'} + 4U_{W'}}{\Delta x^2} + \varepsilon_{yC}\frac{4U_{N'} - 8U_{C'} + 4U_{S'}}{\Delta y^2}\right)\Bigg\}
\end{aligned}
$$

in which

$$
\frac{\partial V}{\partial x}\bigg|_{C'} = \begin{cases} \dfrac{V_{C'} - V_{WW'}}{\Delta x} & \text{if } U_{C'} > 0 \\ \dfrac{V_{EE'} - U_{C'}}{\Delta x} & \text{if } U_{C'} \le 0 \end{cases} \tag{12}
$$

and

$$
\frac{\partial V}{\partial y}\bigg|_{C'} = \begin{cases} \dfrac{V_{C'} - V_{SS'}}{\Delta y} & \text{if } V_{C'} > 0 \\ \dfrac{V_{NN'} - V_{C'}}{\Delta y} & \text{if } V_{C'} \le 0 \end{cases} \tag{13}
$$

From the linear interpolation,

$$
\begin{aligned}
&V_{E*} = (V_C + V_E)/2,\ V_{W*} = (V_W + V_C)/2,\\
&V_{N*} = (V_N + V_C)/2,\ V_{S*} = (V_S + V_C)/2,\ V_{C*} = V_C,\\
&V_{WW*} = V_W,\ V_{EE*} = V_E,\ V_{SS*} = V_S,\ V_{NN*} = V_N,\\
&\eta_{N*} = \eta_N,\ \eta_{S*} = \eta_C,\ U_{C*} = (U_N + U_W)/2,\\
&d_{C*} = (d_C + d_N)/2,\ S_{yyN*} = S_{yyN},\ S_{yyS*} = S_{yyC},\\
&S_{xyE*} = (S_{xyN} + S_{xyE})/2,\ S_{xyW*} = (S_{xyN} + S_{xyW})/2,\\
&\tau_{wyC*} = (\tau_{wxN} + \tau_{wxC})/2,\ \tau_{byC*} = (\tau_{bxN} + \tau_{bxC})/2,\\
&\text{and } \varepsilon_{xC*} = (\varepsilon_{xN} + \varepsilon_{xC})/2,\ \varepsilon_{yC*} = (\varepsilon_{yN} + \varepsilon_{yC})/2
\end{aligned}
\tag{14}
$$

The Q-tree grid is firstly generated and each cell's local configuration identified. Initially, U, V and η are set to zero, and the wave parameters (P, Q and a) are derived from Snell's law. No-flow conditions are applied to the offshore (inflow) boundary in the current field. Offshore boundary values for the wave variables are determined from $a_C = H_o/2$, $P_C = K_E \cos\theta_E$, and $Q_C = [(K + K_N)/2] \sin[(\theta + \theta_N)/2]$ where the non-subscripted variables are determined at the boundary, and H_o is the wave height in deep water. At the onshore boundary, the no-flow condition is imposed. Periodic conditions are applied at lateral boundaries to simulate an infinitely long beach. A simple moving shoreline boundary scheme suggested by Birkemeier and Dalrymple (1976) is implemented in the present model, although special flooding effect is not considered. In practice, the time step is determined by trial and error, and is smaller than the 2-D Courant stability criterion. The separation factor k is calculated either by a Padé form explicit method, ignoring current effects (Hunt, 1979).

5. RESULTS

The present model has been used to evaluate the

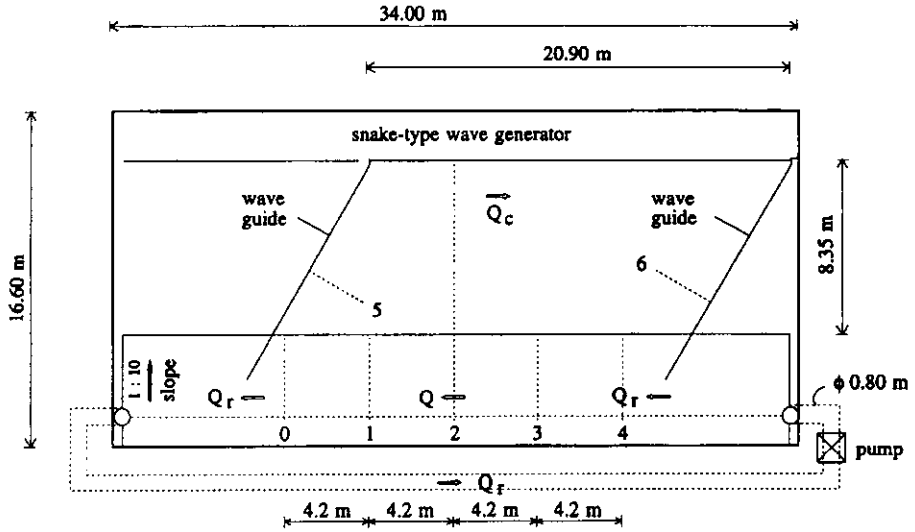

Fig. 4. Wave basin configuration of Vissers experimental set-up.

longshore current induced by waves propagating at a plane beach, for comparison with Visser's (1980, 1991) experimental measurements in a basin 34 m long, 16.6 m wide and 0.68 m deep rectangular tank (see Fig. 4). Visser obtained experimental data on wave-induced currents at 1:10 plane concrete beaches. At the wave generator, the still water depth is 0.399 m.

The offshore wave conditions are height $H_o = 0.071$ m and period $T = 2.01$ s with oblique wave angle of incidence $\theta_o = 31.6°$. The plane beach slope is 0.101.

A uniform mesh is used, composed of 32×32 cells (see Fig. 5). The numerical domain is 3.2 m in both the x- and y- directions. A time step of 0.015 seconds is used for numerical stability, which is much less than the Courant limit. The minimum depth criterion is 0.01 m. To eliminate seiching effects, the wave height is built up over $T_s = 10$ seconds and wave-current is not interacted until $T_{cur} = 10$ seconds. A periodic lateral boundary condition and US-CERC (1984) breaking criterion are applied.

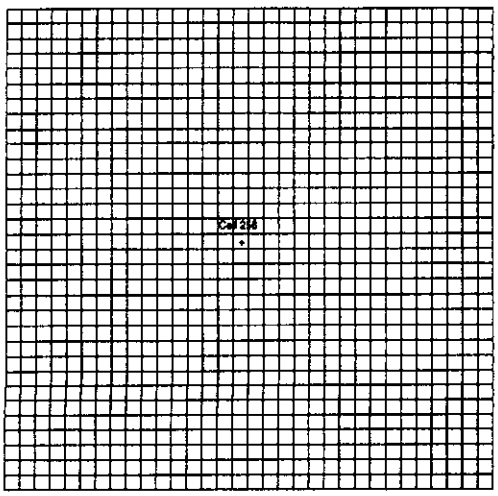

Fig. 5. Fixed mesh for Visser plane beach.

Thornton's (1970) formula provides an estimate of the eddy mixing coefficient as follows

$$\varepsilon_x = M_T A_b U_b$$

where A_b is the wave excursion length at sea bottom and U_b is the maximum wave velocity at sea bottom and M_T is a coefficient. A refined modelling system has already been developed by Yoo and Kim (1994) for the accurate estimation of eddy viscosity using κ-l turbulence closure. But in this study major interest is focused on the application of quadtree system, and relatively simple approach of Thornton formula was adopted for the estimation of eddy viscosity. Until $t = 20$ s, the dimensionless constant, M_T, is 1.0, and then it is linearly decreased to 0.12 from $t = 20$ to $t = 30$ s, held constant at 0.08 until $t = 40$ s, and finally set to 0.05. The bed roughness height R_h is set to 0.01m until $t = 20$ s, and then linearly decreased to 0.0005 m at $t = 40$ s, and this value used thereafter. Fig. 6 presents the oblique wave-induced velocity vectors at 200 seconds.

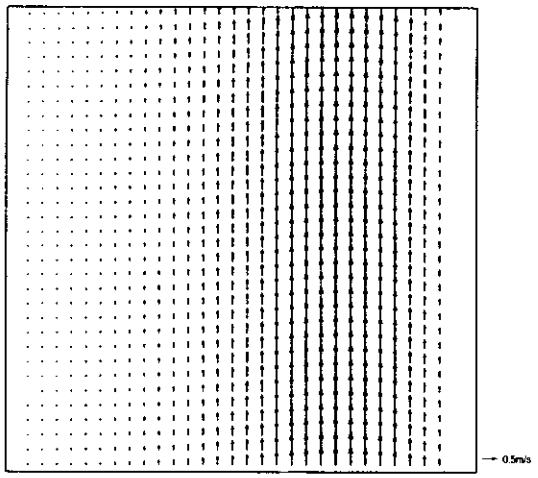

Fig. 6. Velocity vectors with cell 256's location marked plane beach.

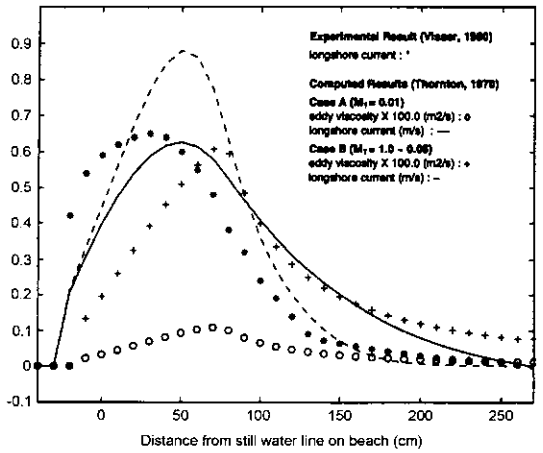

Fig. 7. Eddy viscosity profiles and corresponding longshore currents for different M_T values.

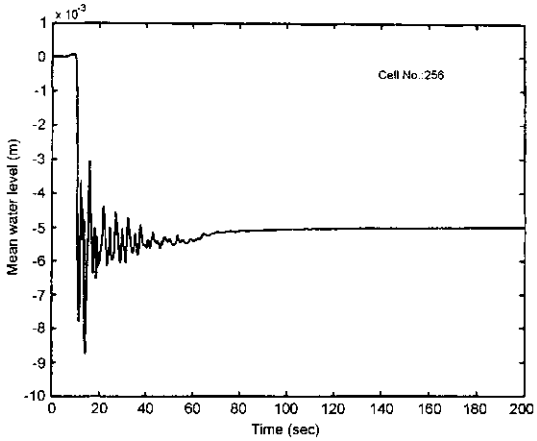

Fig. 8. Predicted mean water level variation as a function of time.

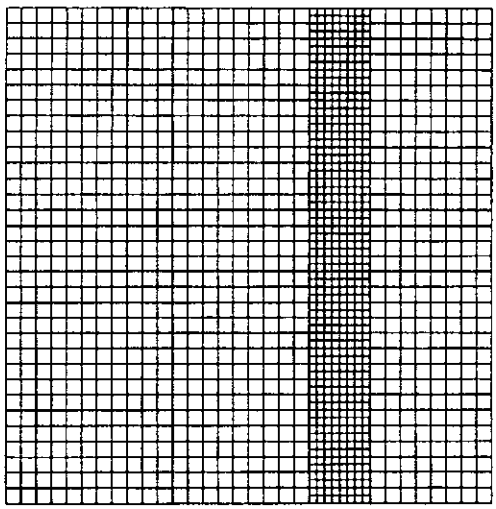

Fig. 9. Adapted mesh for Visser's plane beach.

To determine a suitable value for eddy viscosity, Cases A, B and C were considered with final values of M_T = 0.01, 0.05, 1.0. Fig. 7 shows the cross-shore profiles of eddy viscosity and longshore current for Cases A and B, along with Visser's (1980) experimental value of longshore current velocity. Case A significantly overestim -ates the longshore current while Case B gives a reasonable result but Case C failed to give a solution due to numerical instability. Therefore, Case B was chosen.

The time variation of surface elevation at Cell 256 reaches steady-state after $t = 80$ s (see Fig. 8). The experimental longshore currents are in good agreement, but shifted horizontally due mainly to the breaking criterion and no implementation of flooding effect. As Larsen and Kraus (1991) explained, the simulation could be improved by considering the plunge point shoreward of the wave beaking location (Komar, 1998). The numerical maximum value of longshore current is 0.66 m/s whereas the experimental result is 0.63 m/s.

The initial uniform mesh was adapted according to the longshore current magnitude, so that cells were enriched for $V > 0.54$ m/s at $t = 150$ s. The final converged mesh is shown in Fig. 9. The computation reached steady-state after $t = 154$ s, with a very similar velocity profile (see Fig. 10) to that obtained on the regular grid. This

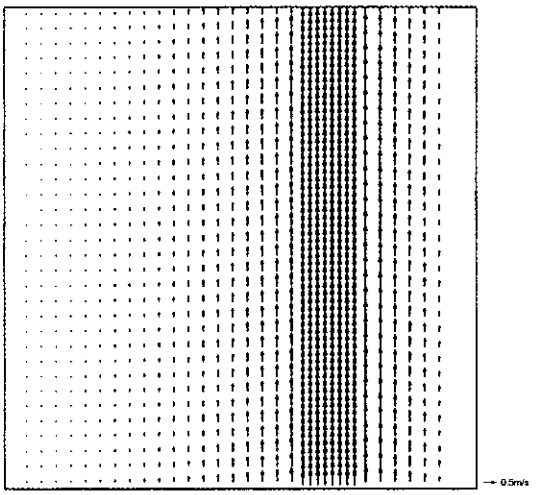

Fig. 10. Longshore current on the adapted mesh.

demonstrates that the present model is able to handle adaptivity, and should be useful in applications involving more complicated boundaries and localised features.

6. CONCLUSIONS

A 2DH numerical model has been developed for predicting nearshore wave-current interaction based on quadtree grids created according to boundary seeding points, which are capable of being locally enriched or coarsened. Grid adaptation criteria can be determined from local flow, bed topography or boundary considerations.

A longshore current was simulated at a plane beach, and the model predictions are compared with experimental data from Visser (1980, 1991). The predictions are convergent and achieve steady-state, with fully developed longshore current pattern in close agreement with the experimental data, except a horizontal shift due perhaps to the breaking criteria used in the numerical scheme and no implementation of flooding effects. Better agreement would be obtained using a wave breaking criterion fitted to the laboratory data. It could also be argued that the wave amplitude cut-off should begin to be applied at the plunge point shoreward of the wave break location (Komar, 1998).

Although it was relatively simple, the test case illustrates that the adaptive quadtree grid approach has a potential for evaluating refined surf-zone hydrodynamics in complicated coastal geometries.

ACKNOWLEDEMENTS

This work was supported by the Hyundai Engineering and Construction Co. Ltd. The author would also like to acknowledge the U.K. Engineering and Physical Sciences Research Council.

REFERENCES

Birkemeier, W.A. and Dalrymple, R.A., 1976. Nearshore water-circulation induced by wind and waves, *Proc. of the Sym. on Modelling Tech.*, ASCE, pp.1062-1081.

Bijker, E.W., 1966. The increase in bed shear in a current due to wave motion, *Proc. 10th Conf. on Coastal Eng.*, ASCE, 746-765.

Ebersole, B.A. and Dalrymple, R.A., 1980. Numerical modelling of nearshore circulation, *Proc. 17th Conf. on Coastal Eng.*, ASCE, **4**, 2710-2725.

Greaves, D.M., and Borthwick, A.G.L., 1999. Hierarchical tree-based finite element mesh generation, *Int. J. for Numer. Methods in Engineering*, **45**, pp. 447-471.

Hunt, J.N., 1979. Direct solution of wave dispersion equation, *ASCE Journal of Waterways, Ports, Coastal and Ocean Engineering*, **105**(WW4), pp. 163-170.

Komar, P.D., 1998. *Beach processes and sedimentation*, 2nd Ed., Prentice Hall, New Jersey.

Larsen, M., and Kraus, N.C., 1991. *MNLONG: Numerical model for simulating the longshore current - Report 1, Model development and tests*, Technical Report DRP-91-1, Dredging Research Program, Washington D.C., U.S. Army Corps of Engineers.

Li, B., 1997. Parabolic model for water waves, *ASCE Journal of Waterway, Port, Coastal and Ocean Engineering*, **123** (4), pp. 192-199.

Mizuguchi, M. and Horikawa, K., 1978. *Experimental study on longshore current velocity distribution*, Bull. Fac. Sci. Eng., Chuo Uniiversity, Tokyo, Japan, **21**, pp. 123-150.

Noda, E.K., 1974. Wave-induced nearshore circulation, *Journal of Geophysical Research*, **79**(4), pp. 4097-4106.

Park, K.-Y., 1999. *Quadtree grid numerical model of nearshore wave-current interaction*, D.Phil. Thesis, University of Oxford, U.K.

Samet, H., 1982. *Neighbour finding techniques for images represented by quadtrees Data Structures*, Computer Graphics and Image Processing, **18**, pp. 37-57.

Thornton, E.B., 1970. Variation of longshore current across the surf zone, *Proceedings 12th Conference on Coastal Engi-*

neering, ASCE, pp. 291-308.

US-CERC, 1984. *Shore Protection Manual,* Coastal Engineering Research Center, Corps of Engineers, Vol. 1,2, Government Printing Office.

Visser, P.J., 1980. Longshore current flows in a wave basin, *Proceedings 17st Conference on Coastal Engineering*, ASCE, pp. 462-479.

Visser, P.J., 1991. Laboratory measurements of uniform longshore current, *Coastal Engineering*, **15**, pp. 563-593.

Yiu, K.F.C., Greaves, D.M., Cruz, S, Saalehi, A. and Borthwick, A.G.L., 1996. Quadtree grid generation: Information handling, boundary fitting and CFD applications, *Computers & Fluids*, **25**(8), pp. 759-769.

Yoo, D.H., and Kim, C.S., 1994. Numerical modelling of longshore currents using k-l turbulence closure, *KSCOE*, **6**(3), pp. 234-244 (in Korean).

Yoo, D., and O'Connor, B.A., 1986. Mathematical modeling of wave-induced nearshore circulations, *Proc. 20th International Conference on Coastal Engineering*, ASCE, pp. 1667-1681.